

Constant chemical potential–quantum mechanical–molecular dynamics simulations of the graphene–electrolyte double layer

Cite as: J. Chem. Phys. **158**, 134714 (2023); <https://doi.org/10.1063/5.0138267>

Submitted: 09 December 2022 • Accepted: 13 March 2023 • Published Online: 04 April 2023

 Nicodemo Di Pasquale,  Aaron R. Finney,  Joshua D. Elliott, et al.

COLLECTIONS

Paper published as part of the special topic on [Chemical Physics of Electrochemical Energy Materials](#)



View Online



Export Citation



CrossMark

ARTICLES YOU MAY BE INTERESTED IN

[MetalWalls: Simulating electrochemical interfaces between polarizable electrolytes and metallic electrodes](#)

The Journal of Chemical Physics **157**, 184801 (2022); <https://doi.org/10.1063/5.0101777>

[Computing chemical potentials of solutions from structure factors](#)

The Journal of Chemical Physics **157**, 121101 (2022); <https://doi.org/10.1063/5.0107059>

[Electrochemistry from the atomic scale, in the electronically grand-canonical ensemble](#)

The Journal of Chemical Physics **157**, 180902 (2022); <https://doi.org/10.1063/5.0123656>



Time to get excited.
Lock-in Amplifiers – from DC to 8.5 GHz

Find out more

Zurich Instruments

Constant chemical potential–quantum mechanical–molecular dynamics simulations of the graphene–electrolyte double layer

Cite as: *J. Chem. Phys.* **158**, 134714 (2023); doi: [10.1063/5.0138267](https://doi.org/10.1063/5.0138267)

Submitted: 9 December 2022 • Accepted: 13 March 2023 •

Published Online: 4 April 2023



View Online



Export Citation



CrossMark

Nicodemo Di Pasquale,^{1,a)}  Aaron R. Finney,²  Joshua D. Elliott,^{3,4}  Paola Carbone,³ 
and Matteo Salvalaglio² 

AFFILIATIONS

¹Department of Chemical Engineering, Brunel University London, Uxbridge UB8 3PH, United Kingdom

²Department of Chemical Engineering, University College London, London WC1E 7JE, United Kingdom

³Department of Chemical Engineering, University of Manchester, Manchester M13 9PL, United Kingdom

⁴Diamond Light Source, Harwell Science and Innovation Park, Didcot, Oxfordshire OX11 8UQ, United Kingdom

Note: This paper is part of the JCP Special Topic on Chemical Physics of Electrochemical Energy Materials.

^{a)}Author to whom correspondence should be addressed: nicodemo.dipasquale@brunel.ac.uk

ABSTRACT

We present the coupling of two frameworks—the pseudo-open boundary simulation method known as constant potential molecular dynamics simulations ($C\mu$ MD), combined with quantum mechanics/molecular dynamics (QMMD) calculations—to describe the properties of graphene electrodes in contact with electrolytes. The resulting $C\mu$ QMMD model was then applied to three ionic solutions (LiCl, NaCl, and KCl in water) at bulk solution concentrations ranging from 0.5 M to 6 M in contact with a charged graphene electrode. The new approach we are describing here provides a simulation protocol to control the concentration of electrolyte solutions while including the effects of a fully polarizable electrode surface. Thanks to this coupling, we are able to accurately model both the electrode and solution side of the double layer and provide a thorough analysis of the properties of electrolytes at charged interfaces, such as the screening ability of the electrolyte and the electrostatic potential profile. We also report the calculation of the integral electrochemical double layer capacitance in the whole range of concentrations analyzed for each ionic species, while the quantum mechanical simulations provide access to the differential and integral quantum capacitance. We highlight how subtle features, such as the adsorption of potassium graphene or the tendency of the ions to form clusters contribute to the ability of graphene to store charge, and suggest implications for desalination.

Published under an exclusive license by AIP Publishing. <https://doi.org/10.1063/5.0138267>

I. INTRODUCTION

Interest in graphene-based devices has grown in recent years thanks to the versatility and physical characteristics of this new material, particularly for applications in which it is in contact with an electrolyte solution. The use of nanoporous graphene as a membrane for water desalination^{1,2} is one important example. The presence of pores of equal size to the electrolytes allows selective passage of water through the membrane. Combined with the atomic-scale thickness of graphene, this can lead to the creation of desalination membranes with higher performances than common polymer-based ones.³ Another promising technologically relevant application is the use of graphene electrodes in electrochemical double layer (super)capacitor (EDLC) devices.^{4–6} In fact, graphene,^{7–10} porous

activated carbon,¹¹ and carbon nanotube^{12,13} electrodes potentially have relatively high charge storage capacity and a favorable specific energy to power ratio due to rapid charge–discharge cycling⁸ controlled by changes of an applied potential together with lifetimes that can reach millions of cycles.¹¹

Typically, charge storage at carbonaceous electrodes is a non-faradaic process, where mobile ionic species accumulate at the interface between the electrode and the liquid phase. An important class of systems of this kind, which has gained lots of attention recently, is represented by cheap and easy-to-prepare aqueous-based electrolytes in contact with a graphene electrode.⁶ Carbon-based EDLCs with aqueous-based electrolytes do not generally suffer from electrochemical degradation, can be nontoxic, and provide an attractive alternative solution to the problem of energy storage compared with

traditional battery devices. Combined with a longer lifetime and high power density,¹⁴ these energy storage systems could be increasingly applied to power small electronic devices and for acceleration and braking in electrical vehicles.⁵

Several experimental works have been undertaken to understand the physicochemical properties of neutral and charged graphene interfaces in contact with electrolyte solutions and to elucidate the nature of their charge storage capacity.^{15–17} However, the delicate balance between hydration-free energy and surface effects, which regulate the physisorption of ionic species at surfaces has resulted in conflicting experimental findings (see Ref. 18 for a more detailed account). For instance, there are reports supporting the conclusion that the capacitance of graphene films is ion-independent¹⁶ as well as contrasting observations suggesting that basal capacitance is instead ion-specific (with, for example, a greater propensity for Na⁺ and K⁺ adsorption over Li⁺ adsorption at negatively charged electrodes in the case of group I cations).¹⁷ Atomic-scale defects in the graphitic surface, its topography, dimensionality, and chemical modifications are difficult to control and have non-negligible effects in experimental measurements. As an example, mechanical cutting produces structural defects known as “dangling bonds,” which modify the measured capacitance of the sample.^{15,19} In this respect, a model of the graphene interface and its interactions with an electrolyte solution can exclude all the spurious effects originating from uncontrolled defects and chemical modification of the surface. Molecular modeling and simulations can help to improve understanding of the mechanisms involved in such complex systems and guide the interpretation of experimental results.

Many key features of supercapacitive devices are underpinned by the properties of the electrochemical double layer and their responses to electrode charging. Gouy–Chapman theory^{20,21} describes a double layer as a diffuse charged layer in the solution that compensates for an applied surface charge on the electrode. Modifications to this model include the adsorption of counterions at the surface in the so-called Stern layer.²² The development of a mean field theory based on the Poisson–Boltzmann lattice-gas model²³ has shown that features absent in the Gouy–Chapman theory, such as steric effects, ion correlations, and preferential adsorption,^{24–26} need to be accounted for in order to correctly describe the interactions between the ions and the electrode. Mechanistic insight for these effects and how they control charge storage can be gained from atomistic simulations of the graphene/electrolyte interface; these also enable the evaluation of ensemble properties, such as the free energy of adsorption of the ions at the interface.²⁷ Furthermore, simulations can establish the effect of solution concentration on ion accumulation at the electrode, their interfacial structure, and their dynamical properties.

In order to compare simulations with a macroscopic system, this adsorption should ideally be modeled in the presence of a bulk electroneutral solution with fixed composition to ensure a constant driving force for the adsorption at a charged surface. The bulk electroneutral solution can be obtained using constant chemical potential MD simulations, *CμMD*,²⁸ which mimics open boundary conditions, as shown in the work of Finney *et al.*²⁹ With *CμMD*, the authors simulated NaCl(aq) with concentrations spanning ~0.1 – 10 M in contact with a graphite surface. Their results indicate that the interface charge screening behavior is a function of bulk solution concentration, with a transition (at ~1 M) from diffuse

charge screening, qualitatively consistent with the picture from simple mean field models to a complex multilayered structuring that systematically either over or under screens the surface potential. The multiple charged layers result from ion finite size effects, overcompensation of the surface charge by oppositely charged ions closest to the surface, and non-idealities in solution, i.e., when the hypothesis of negligible ion-ion interactions breaks down for large ion concentrations.³⁰ This last effect also has consequences for the solution conductivity, which deviates from the prediction of the Nernst–Einstein equations.³¹

Together with a constant driving force for ion adsorption from the bulk, another important effect to consider is the polarization of electrodes exerted by the adsorbing electrolytes.¹⁸ Classical simulations typically model the nonbonded interactions between atoms within the electrolyte and atoms belonging to the interface using additive pairwise potentials such as the Lennard-Jones potential and Coulomb interactions between fixed point atom charges. Polarization can be introduced using, e.g., oscillating charge models or by fitting short-range potentials to binding energies obtained from *ab initio* methods.^{27,32,33} However, these models may not accurately capture the complex many-body effect associated with charge polarization at the electrode–solution interface. Another way to include polarization in classical MD simulations is through the constant potential (CP) method first proposed in Ref. 34 and now popularized by the MetalWalls code.³⁵ The constant potential method has been successfully deployed to describe the properties of the electrochemical double layer of aqueous electrolytes and ionic liquids in contact with metal electrodes such as Au and Cu, nanoporous carbon electrode,^{36,37} and nonplanar electrode.¹⁴ However, without further adaptations, the CP model relies on the approximation that the electrode is metallic and therefore able to perfectly screen charges, which is not the case for (semimetallic) graphene.¹⁸ In recent advances, the Thomas–Fermi model was added to the CP model to tune the metallic character of the electrode allowing the description of imperfect conductors such as graphite.³⁸ Another advantage of the CP-related methodologies is the more straightforward connection with electrochemical experiments, which are usually run by fixing the potential difference of the electrodes.⁶

Despite their successes, all these models rely on classical approximations. In order to describe quantities such as the density of states and electron density distribution in the presence of electrostatic potential arising from electrolyte configuration, we must include some electronic structure theory in the calculations. Though more computationally expensive than a fully classical model, such calculations are needed to determine quantities otherwise inaccessible using a fully classical model. Since there is no one-size-fits-all model, the preferred simulation scheme will depend on the system and available resources, having clearly in mind the strengths and limitations of the different approaches.

A full quantum mechanical (QM) treatment of the interactions between the electrolyte and the substrate is still unfeasible due to the length (tens of nm) and time (hundreds of ns) scales required for modeling the effect of the aqueous electrolytes. However, while the full QM model of the electrode/electrolyte system is out of reach, QM calculations can be used to compute a set of atomic partial charges on the electrode in the presence of electric fields arising from the position of electrolyte atoms. This is exactly the spirit of our

quantum mechanics/molecular dynamics (QMMD) scheme, where QM calculations are coupled to MD simulations at fixed intervals of time integration. As such, the surface atom partial charges within the classical force field are updated on the fly. Such a QMMD scheme does not require any system dependent modification to be applied for a specific system, as shown in Ref. 39, where the QMMD scheme was used without substantial variations for organic polymeric materials. In a more recent development, machine learning models have proven to be a viable option in tuning the surface polarization if the scope of the system becomes too large for QM simulations. This is achieved by replacing the QM calculations with a Neural Network (NN) model trained to reproduce results from a wide range of QM calculations with varying distributions of electrolytes in solution. The NN acts as a polarizable-like force field, combining fast classical MD simulations with more accurate QM calculations of the interface polarization.⁴⁰

This work leverages the QMMD framework introduced in Ref. 18 and the $C\mu$ MD introduced in Refs. 28 and 29. The approach simultaneously captures surface polarization and concentration effects that can modify the structure and composition of the electrochemical double layer. We use the resulting $C\mu$ QMMD protocol to examine interfaces between aqueous alkali chloride solutions at different concentrations with a graphene electrode surface, elucidating complex interfacial structure, dynamics, and electrochemical properties.

This paper is organized as follows: We first provide a brief overview of the QMMD and $C\mu$ MD protocols, pointing to the relevant literature for the interested reader; we present the systems to which we apply the $C\mu$ QMMD framework: a charged graphene electrode in contact with three different electrolyte solutions, NaCl(aq), LiCl(aq), KCl(aq), at different concentrations. We derive the electrical properties of the interface in terms of the screening factor and electrical potential and calculate the total integral capacitance of this system by deriving the quantum and electrical double layer capacitance. Finally, we discuss the effects of complex solute speciation on the performance of graphene-electrolyte devices and draw some conclusions regarding this newly proposed simulation scheme.

II. COMPUTATIONAL MODELS

In order to capture the dynamic polarization of a charged graphene surface in response to the evolving configuration of an electrolyte at a prescribed concentration, we coupled the classical $C\mu$ MD simulation to the electronic structure theory calculations at regular time intervals. We provide a more detailed account of both models ($C\mu$ MD and QMMD) in the following sections, while here, we will only discuss their coupling.

A sketch of the sequence of the operations involved is given in Fig. 1. All the operations shown in Fig. 1 are obtained through an in-house python wrapper. During the MD time integration obtained with GROMACS 2018.4 MD package,⁴¹ ion positions are passed to the Plumed software (v. 2.7)⁴² patched with GROMACS, to compute the $C\mu$ MD forces (see Sec. II A for more details). After the evolution of the atom positions, the final configuration of the electrolyte is extracted to compute the electrostatic potential. In turn, this latter quantity is used as input for the QM calculations obtained with the DFTB+ software package.⁴³ A more detailed description of the QM calculations is reported in our previous publications.^{18,44} From the

QM results, the distribution of charges on the graphene is extracted (see Sec. II B for more details) and used as input for the new iteration of the loop.

A. $C\mu$ MD model

The graphene electrode we considered is located at $z = 0$ and is in contact with an electrolyte slab of thickness 8 nm. A further 8 nm of vacuum separates the system from its periodically repeating images. The electrolyte phase is divided into three regions: The first region starts at the graphene electrode up to a distance of 4 nm. The second one is the *control region*, where the solution composition is fixed. The third region is the *reservoir region*, which provides the reservoir of ions to adjust the concentration of the electrolytes in the other regions. Figure 2 provides an example of the setup adopted in this work, where we highlight the different $C\mu$ MD simulation cell regions.

The control of the concentration of ions in solution is obtained by applying a force at the edge of the reservoir region according to a continuous function of the form

$$F_i^H(z) = k_i(n_i^{\text{CR}} - n_i^0) \left[\frac{1}{4\omega} \left(1 + \cosh\left(\frac{z - z_F}{\omega}\right) \right)^{-1} \right]. \quad (1)$$

Here, ω was set to 0.2 nm and represents the width of the force region (between the control and reservoir regions highlighted by the blue lines in Fig. 2), while k was 2×10^4 kJ mol⁻¹ nm⁻¹, giving the correct densities in the bulk (see Ref. 29 for a discussion on these parameters). n^0 is the target ion number density, while n^{CR} is the density calculated instantaneously during time integration in the control region. Finally, z_F is the position in z where the $C\mu$ MD forces are applied. In our simulations, this is set to 5.5 nm beyond the graphene surface. Using this approach, the densities of cations and anions are constrained in the control region to maintain target concentrations of 0.5, 2.0, 3.0, 4.0, 4.4, and 6 M. At each MD time step, ion positions are passed to Plumed in order to compute the $C\mu$ MD forces only acting on those ions in the region of z_F . No external forces are applied to the ions outside this region, and any local change in the ion density at the interface results from the physical interactions between graphene and the solution.

B. QMMD model

The generality of electronic structure theory and its ability to reproduce the electronic charge density distribution in semiconductors, metals, and semimetals implies that the QMMD approach can describe both long- and short-ranged redistribution of the surface charge induced by the presence of the electrolyte. Within each iteration of our scheme (see Fig. 1), the fully classical system is taken as input for a quantum mechanical calculation. The simulation box is partitioned into surface atoms whose electronic structure is explicitly treated and electrolyte atoms that are converted into a set of point charges. The point charges take the values of the partial charges contained in the classical force field and form the background electrostatic potential during the computation of the electron structure (a sketch of this step is presented in Fig. S1 of the supplementary material).

In order to describe the electronic structure of solid–electrolyte interfaces on the length scales required, we leverage the self-consistent charge Density Functional Tight-Binding (SCC-DFTB)⁴⁵

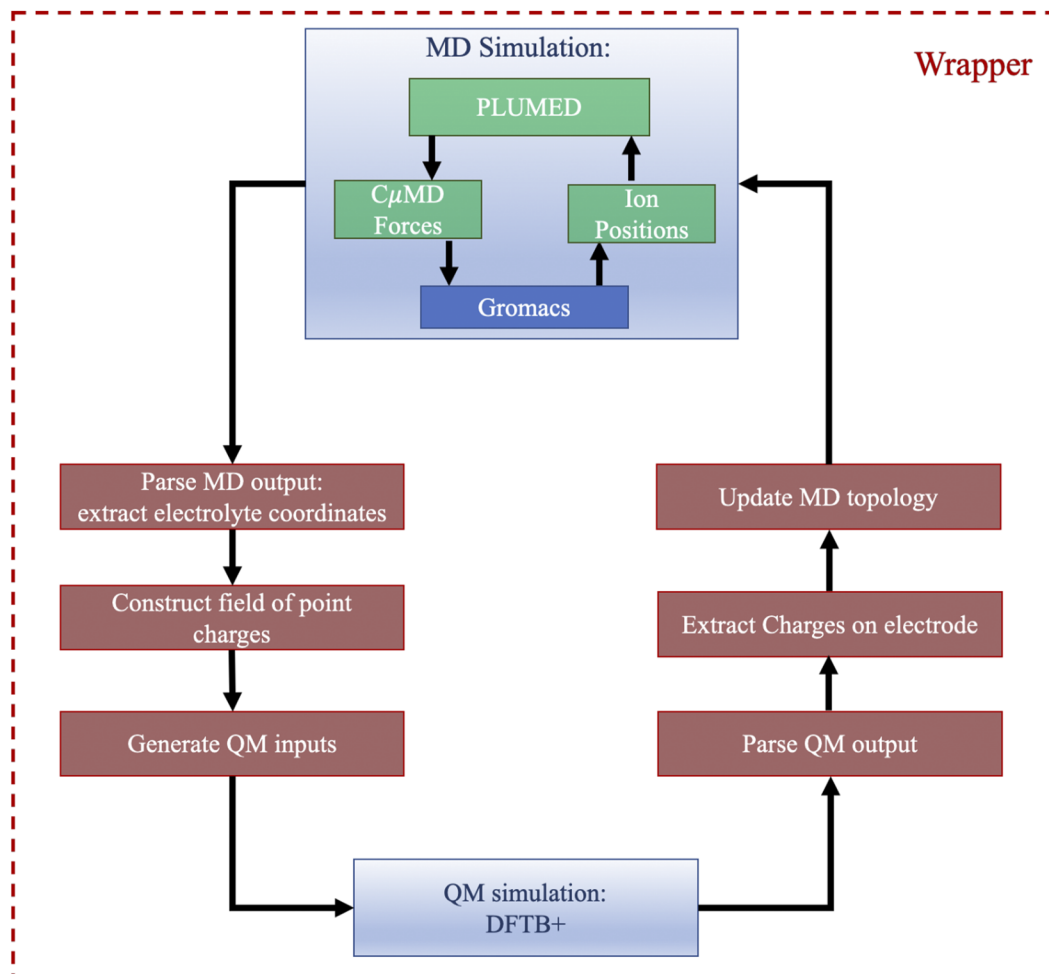


FIG. 1. A representation of the computational workflow adopted in this work. The blue squares indicate the MD software and the QM software we adopted, which, for the purpose of the python wrapper are called external programs (i.e., we just take them as “black boxes”), whereas the red squares highlight the operations included in the python wrapper.

approach, which is an approximation to Kohn–Sham Density Functional Theory.

Upon derivation of the electronic structure, partitioning the charge density via Mulliken population analysis yields the surface atom partial charges, which are then passed to the classical force field. Finally, a short MD trajectory on the order of several picoseconds can be carried out (in the presence of the quantum mechanically polarized surface) to generate the electrolyte configuration for the following iteration. In our simulations, we employ a coupling between QM and MD calculations of 5 ps. We previously found for this class of systems that 5 ps represents a good compromise in terms of computational accuracy of the computed charges ($0.004 e$) vs computing time when compared with a QMMD simulation where the charges were updated at every MD time step.¹⁸

C. Simulations details

We will give in this section an account of the systems simulated, along with the numerical parameters considered in our work.

In our simulations, we consider a graphene electrode composed of 336 carbon atoms in contact with aqueous electrolyte solutions. We investigated three electrolyte systems, NaCl, KCl, and LiCl, at concentrations ranging from 0.5 to 6 M. However, due to the solubility limits of the KCl(aq),^{46,47} we limit the investigated concentrations to 4.4 M for the KCl system. These were target concentrations for the control region, which we refer to throughout when discussing each system. An accurate evaluation of the bulk concentration requires sampling the mean ion density values in z far from the interface. At most, the deviation of the evaluated concentrations from the target ranges from 0.1 to 0.26 M across the concentration range we considered.

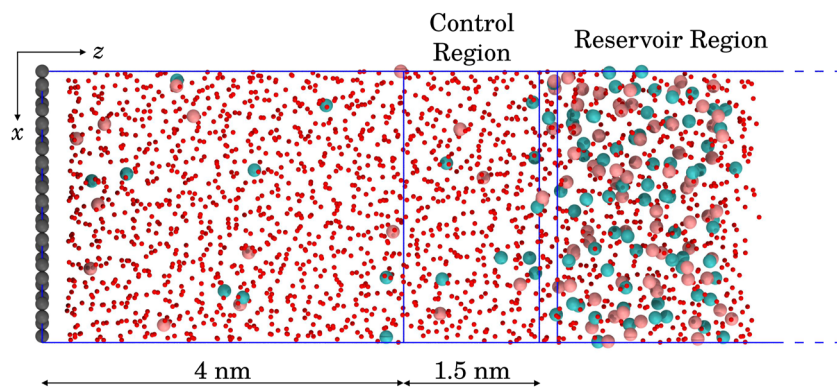


FIG. 2. Example configuration from a $C\mu$ QMMD simulation of $KCl(aq)$ in contact with graphene in this work projected onto simulation x, z dimensions. K^+ , Cl^- , O of water and C of graphene are shown by pink, cyan, red, and gray spheres. The blue lines highlight the $C\mu$ QMMD control and reservoir regions, which also indicate the simulation cell boundaries. An extended vacuum region, around 8 nm in z , is truncated in the image.

Our simulations are carried out at constant surface charge, which makes it difficult to draw comparisons across different electrodes since the potential applied is not necessarily constant. As such, when we compute the capacitance, we use the potential drop of the neutral electrode as a reference. This approach has been applied previously to compare the properties of the electrochemical double layer for different electrolytes.⁴⁸ Each operating condition was therefore repeated for two different total charges of the electrode: a charged graphene layer with a constant charge on the surface⁴⁹ σ of -0.449 e nm^{-2} (-0.0719 C/m^2) and a neutral one ($\sigma = 0$). In cases where $\sigma = 0.449 \text{ e nm}^{-2}$, this corresponds to an overall charge on the electrode of -4 e ; we accordingly added four cations to the system to compensate this surface charge.

It is important to highlight here that the whole loop represented in Fig. 1 requires the interaction among three different software packages, Gromacs,⁴¹ PLUMED,⁴² and DFTB+,⁴³ and we will describe here the relevant parameters required in each case.

As described in Sec. II B, in the QM part of the loop, we perform DFTB calculations, which are obtained here using the DFTB+ software package.⁴³ The empirical description in our DFTB+ calculations of the interactions between the C atoms in the surface are described by the mio-1-1 parameter set.⁴⁵ The SCC charge threshold and Fermi temperature have been set to 1×10^{-2} Hartree and 300 K, respectively. Whereas, on first inspection, these criteria can be considered loose and should not be adopted for the calculation of the total electronic energy, rigorous testing in our previous studies^{18,44} found that they provide a sufficiently accurate description of the surface charge distribution with respect to fully converged simulations, at a fraction of the computational cost. Finally, to compute the partial charges passed to the graphene force field at each MD step, we perform a Mulliken population analysis,⁵⁰ which gives reasonable results for this class of systems.^{18,44} Mulliken charges ensure full equivalence between the DFTB and classical forces acting on the electrolyte atoms as we verified in our previous work.¹⁸

Molecular dynamics calculations in the NVT ensemble are carried out using GROMACS,^{51,52} version 2018.4. The leapfrog algorithm with a time step of 1 fs was used to integrate the equations of motion at a constant temperature of 298.15 K, controlled with the Nosé–Hoover thermostat, with a relaxation time of 1 ps. Long-range electrostatic interactions were treated using the particle-mesh Ewald approach, with a cutoff of 1.4 nm. Nonbonded interactions were computed using a Lennard-Jones 12–6 potential, truncated

smoothly at 1.0 nm using a switch function starting at a distance of 0.99 nm. In all simulations, graphene carbon atoms were frozen, and water was modeled using the SPC/E model⁵³ with the SETTLE algorithm used to maintain rigid molecule geometries.⁵⁴ This choice is compatible with the Werder water–graphene parameters that reproduce the experimentally measured graphene/water contact angle.^{7,55} Ion force field parameters (for K^+ , Li^+ , Na^+ , Cl^-), also compatible with the SPC/E model, are taken from the work of Joung and Cheatham.⁵⁶ At the beginning of time evolution, in systems at the higher end of the concentration range, many ions need to be stored in the reservoir. This occasionally led to water molecules escaping into the vacuum region due to close ion-ion contacts. Additional relaxation steps could be used to avoid these spurious effects; however, we added a fixed wall above the reservoir, interacting with water molecules and ions only through a short-range Lennard-Jones potential.

We equilibrated each system for 20 ns followed by 130 ns production runs to collect data for subsequent analyses of the steady-state structure of the interface. In all analyses discussed below, mean values and standard deviations (error bars) are obtained via averaging performed using 5 ns windows.

Structural analyses of the solutions are carried out using PLUMED⁴² by post-processing the simulation trajectories. The first-shell coordination numbers are given by N_{X-Y} , where $X = \{Na^+, Li^+, K^+\}$ and $Y = \{Ow, Cl^-\}$. Therefore, N_{X-Cl} represents the first-shell coordination numbers for cations with anions, and N_{X-Ow} is the same quantity for cations with water oxygen atoms. N_{X-Y} is computed as $N_{X-Y} = \sum N_{X-Y}^i$ where the index i indicates the i th anion or water oxygen atom depending upon the type of coordination number being evaluated. In turn, N_{X-Y}^i is defined using a switching function for distances larger than d_0 ,

$$N_{X-Y}^i = \begin{cases} e^{\left(\frac{-(r_i-d_0)^2}{2r_0^2}\right)} & \text{if } r_i > d_0, \\ 1 & \text{otherwise,} \end{cases} \quad (2)$$

where r_i are distances between pairs of atoms, $r_0 = 0.01 \text{ nm}$, and d_0 is the distance between a cation center and the first minimum in radial distribution functions for the cations with anions or water oxygen atoms. We report radial distribution functions for the different systems considered in Fig. S2 of the [supplementary material](#),

from which we obtained $d_0 = 0.29, 0.34,$ and 0.39 nm for Li–Na– and K–Cl. This ensured that a conservative definition of first-shell coordination was adopted in the analyses. Coordination numbers were evaluated in 1.3 nm regions in z closest to the graphene surface and 3.5 nm from the surface, representing the double layer and bulk solution regions, respectively. The first coordination sphere distributions for ions were used to construct a graph of ion–ion contacts using the NetworkX Python library.⁵⁷ This allowed us to identify and compute the size of the ion clusters formed. Ion clusters at the interface and within the bulk were identified by sampling the regions defined for computing the coordination numbers. Clusters were identified as fully connected networks in the graph of adjacent ion–ion connections according to this geometric criteria, regardless of their total charge or lifetime.

III. RESULTS AND DISCUSSION

Thanks to the simulation protocol implemented, electroneutral solutions with fixed ion concentrations can be maintained in the Control Region as shown in Fig. 2, representing bulk solutions in equilibrium with the electrode–solution interfaces. This allows us to compare the behavior of different electrolytes while controlling the electrolyte background concentration.

A. Density profiles

We start this section by reporting in Fig. 3 the (molar) concentration of the different ionic species in solution as a function of the z coordinate, corresponding to the simulation cell direction orthogonal to the surface of negatively charged graphene electrodes. As expected, these profiles show preferential adsorption of cations at the electrode surfaces. For Na^+ and Li^+ , a sharp density peak is observed at a distance of 0.5 nm from graphene, followed by a second, less pronounced peak at 0.75 nm. At the highest concentrations, a third cation peak emerges around 1.15 nm, which is more pronounced for Li^+ . In contrast, in the case of K^+ , a small peak at 0.3 nm is followed by a much larger and relatively diffuse density peak at 0.6 nm. This is due to specific adsorption of the larger cation at the carbon surface, a small number of which partially dehydrate to directly coordinate to carbon.

The difference in the z -density profiles for the different systems is less notable when considering Cl^- with respect to cations. At the lowest bulk concentrations, there is a monotonically increasing density, which reaches bulk values around 1.5 nm from the graphene interface. As the concentration rises, further density peaks are observed close to the carbon substrate, determined by the emergence of a multilayered electrical double layer structure, consistent with previously reported results.^{18,29} In such double layer configurations, adjacent solution layers, rich in cations or anions, arise at the interface due to ion crowding (as in the case of the cations that are attracted toward the negatively charged surface of the electrode) and ion correlation (the localized positive excess charge in the closest layers to the electrode, in turn, attracts the anions).

The results reported in Fig. 3 are consistent with those of Ref. 44 with NaCl(aq) and LiCl(aq) systems displaying, qualitatively, the same solution side double layer structure. The case of KCl(aq) differs somewhat. While the positions of the first two peaks [at 0.3 and 0.6 nm, see Fig. 3(c)] that we obtained in our work is the same

as the ones obtained in Ref. 44 for an analogous system, the intensity is different. In particular, our model predicts the majority of the K^+ are residing in the outer Helmholtz layer with a minority being absorbed on the interface, while results reported in Ref. 44 show that the majority of the K^+ are instead absorbed on the interface, and few of them reside in outer Helmholtz layer. This difference in the intensity of peaks reflects the difference of the classical force field used, in particular related to the fact that the force field considered in Ref. 44 (i.e., the Madrid-2019 Force-Field⁴⁷) considers scaled ionic charges and the K^+ ions have a lower solvation free energy than the K^+ modeled with the force field considered in this work.⁵⁸ The reduced strength of the interactions between the potassium and the water in the Madrid-2019 force-field makes the K^+ cation described in Ref. 44 more susceptible to dehydration and, therefore, more likely to be adsorbed on the graphene.

Key differences between the adsorption behavior of the ions is captured when polarization of the electrode is accounted for. We have demonstrated this for two different force fields (here and in Ref. 44), which suggests that the behavior is independent of the classical models. We note, however, that while qualitatively similar, the different classical force fields lead to different quantitative adsorption intensities of the K^+ ion on the surface—which can be linked to their slightly different classical free energies of hydration and ionic charge. On the other hand, other results in the literature (see Ref. 59) show clear qualitative differences with our simulations [in particular for the KCl(aq) system where no adsorption is observed], most likely due to the lack of dynamic polarization considered for the graphene electrodes.

In turn, this brief account of the results in the literature shows the subtleties of discarding the polarizable nature of the electrode. Whenever polarization is considered, we observe the adsorption of K^+ , implying that a nonpolarizable model needs to be thoroughly checked, as it can change the physics of the model.

B. Electrical double layer properties

In this section, we derive and analyze the electrical properties of the electrode–electrolyte systems considered in this work.

1. Electrode charge screening

We begin by considering the screening factor²⁹ f defined as

$$f(z) = - \int_0^z \frac{\rho_{\text{ions}}(z')}{\sigma} dz', \quad (3)$$

where σ is the surface charge of the electrode interface and $\rho_{\text{ions}}(z)$ is the charge density of ions only, which is considered a function of just the z coordinate, i.e., it is averaged over the x and y coordinates.

The screening factor represents the extent to which the electrolyte phase electrically screens the charged interface. When f converges to a value of one, the charge on the electrode is entirely shielded by the electrolyte. Here, we include only the charges on ions when computing the solution charge density in z to facilitate a comparison with simple mean field models, which often treat the solvent as a continuum field with defined permittivity. However, we report the screening factor calculated using the total charge density in Figs. S19–S21 and Sec. S2 of the [supplementary material](#).

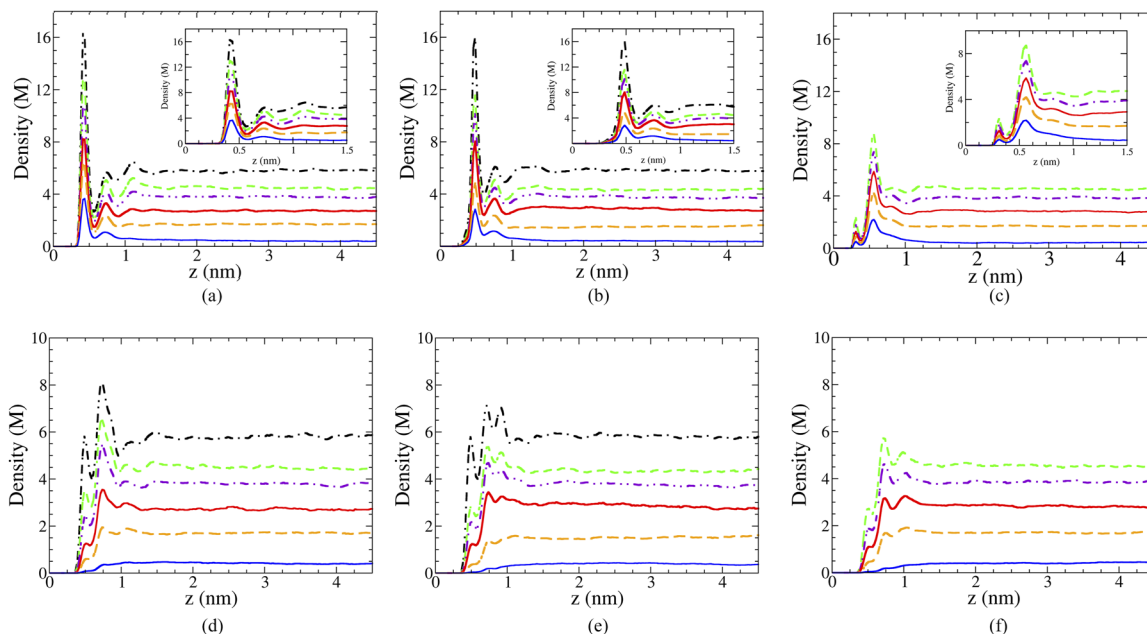


FIG. 3. (a) Li^+ , (b) Na^+ , (c) K^+ , (d) Cl^- in $\text{LiCl}(\text{aq})$, (e) Cl^- in $\text{NaCl}(\text{aq})$, (f) Cl^- in $\text{KCl}(\text{aq})$. Molar (M) density of the cations (top row) and the corresponding anions (bottom row) for the three systems considered in this work. In the insets, the same results are shown for the region at 1.5 nm from the graphene electrode. The different curves are indicated as follows: Black dashed–dotted curve for a concentration of 6 M, green short-dashed curve for a concentration of 4.4 M, magenta double dotted–dashed curve for concentration of 4.0 M, solid red curve for a concentration of 3.0 M, orange long-dashed curve for a concentration of 2.0 M, and a solid blue curve for concentration of 0.5 M, respectively, where concentration refers to the bulk solution concentration. The color code defined here will be valid for all the results shown in Secs. III A and III B. We report the same pictures with error bars in Figs. S3–S8 of the [supplementary material](#).

The screening factors for all systems are reported in Fig. 4. When the concentration of the ions is below 1 M, an under-screening near the interface can be observed. The screening factor f increases smoothly, reaching the value of one at around $z = 2$ nm. This is qualitatively consistent with the predictions of Gouy–Chapman’s theory, where a diffuse double layer region with exponentially decreasing and increasing counterion and co-ion concentrations is predicted as a function of a monodimensional distance

coordinate adjacent to a charged, planar surface. For higher concentrations, however, f transitions to over-screening at relatively small values of the z coordinate. The over-screening, highlighted by the first peak at $z \approx 0.6$ nm reported in Figs. 4(a)–4(c), depends both on the particular ion and on the bulk concentration. In particular, the LiCl system has the strongest over-screening effect on the electrode across the entire concentration range considered. When all solution charges are included in the determination of $\rho(z')$ in

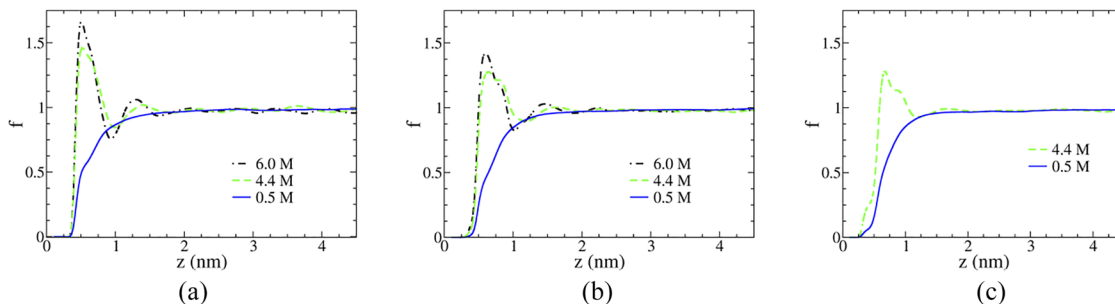


FIG. 4. (a) LiCl , (b) NaCl , (c) KCl . Screening factor as defined in Eq. (3) for the three systems considered using ions charge densities only. We included only a subset of the concentrations without error bars for clarity. The color scheme follows the convention defined in Fig. 3. The results for all the concentrations along with error bars are reported in the [supplementary material](#) (see Figs. S9–S11 of the [supplementary material](#)).

Eq. (3), as shown in Fig. S20 of the [supplementary material](#), the over- and under-screening in the double layer are amplified, highlighting how the structuring of both ions and solvent and the finite size of molecules in solution layers should be included to properly account for the screening of the surface potential by the solution.

Over-screening is a well-known effect for ionic liquids²⁵ and is usually not considered important in electrolyte solutions as this was only apparent at relatively high concentrations.^{18,29,59} The fact that over-screening appears for a higher concentration of the solute, in turn, can be linked directly to the structuring of ions near the interface observed in Fig. 3. At increased ion concentration, the density of cations close to the electrode increases with respect to their value in the solution bulk (see Fig. 3). The excess charge associated with this ion accumulation is balanced in adjacent solution layers until the average bulk density is reached.¹⁴ This description is consistent with our observations, where lithium and sodium show a high degree of structuring near the interface relative to potassium (i.e., multiple ion density peaks are observed, accompanied by a significant over-screening effect). In contrast, potassium, with the lowest degree of structuring near the interface, shows the smallest over-screening among the three ion solutions considered. Moreover, for potassium, we observe a variation in the slope of the screening factor when $z \approx 0.5$ nm, which increases (becoming more pronounced) as a function of concentration. This additional feature in the screening factor, absent in NaCl and LiCl, can be explained by the direct coordination of the K^+ (i.e., through the first coordination sphere) to carbon atoms (as also observed in Ref. 44), as opposed to the behavior of the cations in LiCl(aq) and NaCl(aq) systems [see the first peak at ≈ 0.35 nm in Fig. 3(c) with respect to the first peak at ≈ 0.5 nm in Figs. 3(a) and 3(b)].

2. Electrode polarization

We will focus in this section on the K^+ ion as it is the only one which is adsorbed on the graphene surface. The solvation free energy of the potassium is the lowest among the three cations.⁵⁸ Therefore, one expects a greater ability of K^+ to lose (at least partially) its solvation shell with respect to Li^+ and Na^+ . However, the smaller free energy by itself does not guarantee to observe the adsorption, as we previously noted in the results reported in Refs. 59 and 60.

In a polarizable model of the interface, the approach of a positively charged ion to the (overall negative) interface greatly influences the distribution of the charges on the surface. In particular, when a cation is adsorbed on the surface, we can expect a stronger localization of negative charges near its position. We give an example of this behavior in Fig. 5 where we show the coordination of the K^+ with the carbon atoms on the graphene electrode for the lowest (0.5 M) and the highest concentration (4.4 M) considered here. The plots in Fig. 5 represent a single snapshot in the 150 ns long simulation with the highest number of potassium cations in direct contact with the interface (i.e., at a distance of 0.26 nm from the interface). As expected, the number of K^+ in direct contact with the interface increases as the bulk concentration of the cations increases, consistent with the observation in Fig. 4 for the short-distance (from the electrode) behavior of the screening factor, which increases with concentration. The accumulation of K^+ at the electrode [see Fig. 3(c)] results in an increased nonuniformity of the partial charge distribution on the electrode, with higher negative

charges located on the carbons closer to the coordinated K^+ .

The feedback mechanisms just described, i.e., a cation with low solvation free energy approaches the interface in the electrical double layer, the localization of negative charges promotes the loss of water molecules, which allows the cation to move closer to the interface, which in turn responds with a stronger localization of the negative charges, is what makes the adsorption possible.

The results we have presented in this section show the importance of including the polarization of the interface in a model to correctly capture the adsorption behavior; however, more studies are needed to put these analyses on a firm quantitative basis. In particular, it would be useful to evaluate the free energy barriers for solvent removal from cation first coordination spheres near charged surfaces.

3. Electrical potential in the double layer

We calculated the electrical field $E(z)$ and the electrical potential, $\psi(z)$, in the direction orthogonal to the interface using the Poisson equation,

$$-\frac{d^2\psi(z)}{dz^2} = \frac{dE(z)}{dz} = \frac{\rho(z)}{\epsilon_0}, \quad (4)$$

where $\rho(z)$ is the charge density calculated for all atoms in the system calculated along the perpendicular axis to the electrode and ϵ_0 is the permittivity in vacuum. The electrical potential, $\psi(z)$, is obtained by integrating Eq. (4) twice with respect to the z coordinate,

$$\psi(z) = -\frac{1}{\epsilon_0} \int_0^z \int_0^{z'} \rho(\zeta) d\zeta dz'. \quad (5)$$

The two integration constants associated with Eq. (5) are chosen to set the electrostatic field and potential equal to zero in the bulk, which amounts to considering the bulk as the reference for the calculation of the electrostatic potential.

The results of Eq. (5) are reported in Fig. 6 for a selection of concentrations (see Figs. S12–S14 of the [supplementary material](#) for the entire range of concentrations). In stark contrast to the exponential behavior predicted by models based on the Gouy–Chapman double layer theory, which treats the solvent medium as a continuum with known dielectric, atom/molecule finite size effects give rise to an undulating $\psi(z)$ function in the interfacial region at all concentrations and in all systems. When calculating the charge distribution, we include all solution species, including the partial charges associated with the oxygen and hydrogen atoms in water molecules. Hence, it is unsurprising that the structuring of ions and water molecules at the interface gives rise to a significant departure from the predictions of simple mean field models. Indeed, these finite size effects are a well-reported feature of electrode–electrolyte systems.^{61,62}

From a relatively large negative value of the potential at the electrode, the (partial) charges of ions and water give rise to fluctuations that attenuate at larger values of z , where the bulk solution behavior is recovered. Generally, increasing the bulk solution concentration increases the amplitude of $\psi(z)$ fluctuations. Furthermore, it is evident from Figs. 6(a) and 6(b) that the crowding of ions in the double layer increases with concentration as the positions of

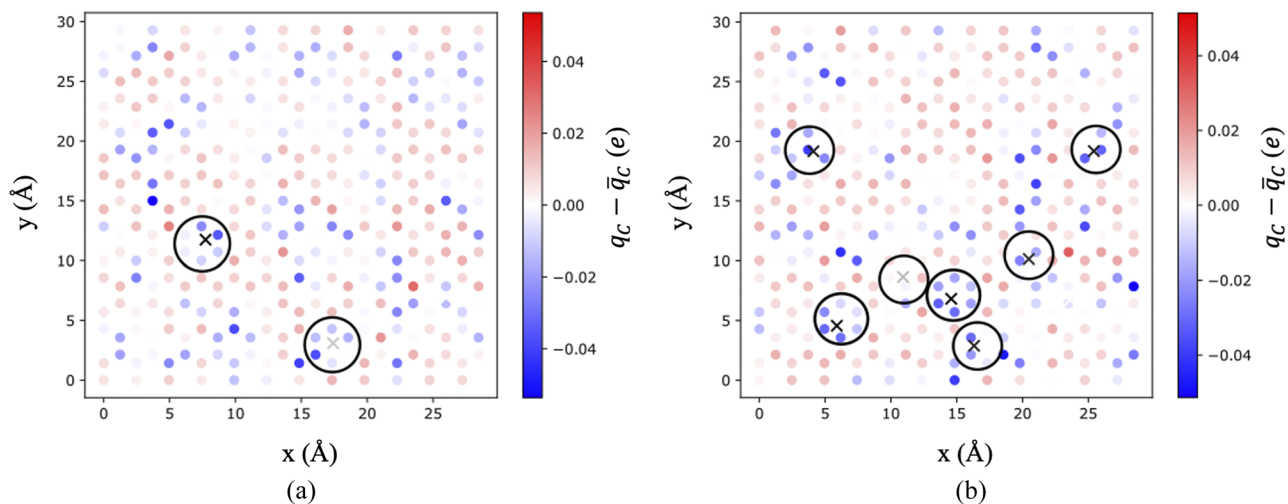


FIG. 5. (a) 0.5 M, (b) 4.4 M. Representative plot of the computed Mulliken charges on the graphene sheet charged with $-4 e$ and in contact with KCl solutions at different concentrations. The results are given in terms of deviation from the average charge per carbon atom (given in this case by $\bar{q}_c = -4/336 e$, where $-4 e$ is the total charge of the graphene sheet composed by 336 carbon atoms). Circled X's mark the coordinates of K ions directly adsorbed on the surface.

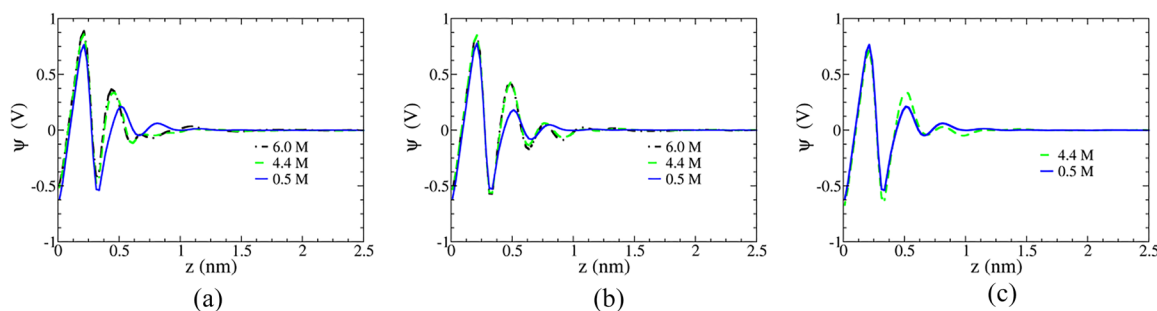


FIG. 6. (a) LiCl, (b) NaCl, (c) KCl. Electrostatic potential as defined in Eq. (5) for the three systems considered at the highest and lowest concentrations for each system. We included only a subset of the concentrations for clarity. The color scheme follows the convention defined for Fig. 3. The results for all the concentrations are reported in the [supplementary material](#) (see Figs. S12–S14 of the [supplementary material](#)).

peaks and minima in z shift to lower values, a feature also observed in the work of Finney *et al.*²⁹ with graphite and which was related to changes in the screening factor. This concentration dependence is less apparent in the case of KCl(aq), where the value of $\psi(z)$ at the first maximum is less susceptible to changes in the concentration as opposed to NaCl(aq) and LiCl(aq).

4. Electrical double layer capacitance

The total capacitance C_{TOT} can be modeled as two independent components combined in series: the Electrochemical Double Layer Capacitance (EDLC), C_{EDL} , and the quantum capacitance (or the space charge capacitance, C_Q), depending on the spatial distribution of the charges on the graphene.⁴⁴ The total capacitance is then given by

$$\frac{1}{C_{TOT}} = \frac{1}{C_{EDL}} + \frac{1}{C_Q}. \quad (6)$$

From Fig. 6, we can easily derive the potential drop, $\Delta\psi$, across the interface as⁴⁴ $\Delta\psi = \Delta\psi^- - \Delta\psi_{ref}$ where $\Delta\psi^-$ and $\Delta\psi_{ref}$ represent the potential drop at the interface with respect to the bulk for the charged and neutral electrodes, respectively. As a reference for the calculation of the potential drop, we use the potential at the interface in a neutral electrode with all other conditions unchanged. We report the calculation of the potential across the system for a neutral electrode in the [supplementary material](#) (see Figs. S15–S17 of the [supplementary material](#)) along with the potential drop at the interface both for the neutral electrode ($\Delta\psi_{ref}$) (see Table S1 of the [supplementary material](#)) and the charged electrode ($\Delta\psi^-$) (see Table S2 of the [supplementary material](#)). With this definition of the potential drop, the EDLC can be obtained, as

$$C_{EDL} = \frac{\sigma}{\Delta\psi}. \quad (7)$$

The quantum capacitance instead is obtained by calculating the differential quantum capacitance C_Q^{diff} according to Ref. 44,

$$C_Q^{diff}(\psi) = \frac{e^2}{4k_B T} \int_{-\infty}^{\infty} [D(E) \operatorname{sech}^2(E + \psi)] dE, \quad (8)$$

where e is the electron charge, E is the energy relative to the Fermi level, $D(E)$ is the density of states at a given energy, k_B is the Boltzmann constant, and T is the temperature. By integrating the differential quantum capacitance with respect to the potential ψ up to the potential drop $\Delta\psi$ calculated for each system, we obtain the integral quantum capacitance C_Q ,

$$C_Q = \frac{1}{\Delta\psi} \int_0^{\Delta\psi} C_Q^{diff}(\psi) d\psi. \quad (9)$$

For more detailed information about the calculation of the quantum capacitance, we refer the reader to our previous work.⁴⁴

The results for C_Q , C_{EDL} , and C_{TOT} for all of the systems considered are reported in Table I. The data show that the total capacitance is practically constant across the entire concentration range and for all solution types. The largest variation in C_{TOT} we obtained among all the systems is $\approx 2\%$ [between LiCl(aq) and KCl(aq) at 4.4 M]. This result contrasts with the different behavior of the three cations in solution and near the electrode interfaces as highlighted in the discussion of the number density of ionic species (see Fig. 3) their screening effect on the charge of the electrode (Fig. 4), and as further discussed in Sec. III C in relation to their clustering properties.

An important point we want to highlight here is that such differences in the behavior of the cation in solution can be correctly captured through the use of a simulation protocol that combines the pseudo-open boundary condition, i.e., $C\mu MD$, to maintain constant composition electroneutral bulk solutions beyond the double layer, and the quantum mechanical description for the distribution of partial charges of the electrode. While capacitance is a critical parameter to determine the suitability of the graphene-electrolyte system as a supercapacitor, this quantity alone fails to delineate the rich interfacial structure and dynamics of ions apparent for different electrolytes.

C. Ion association

An often overlooked effect in alkali chloride solutions is the tendency for ions to associate, forming clusters. Depending upon the operating conditions, these effects may have important implications when designing charge storage and desalination devices. Furthermore, a molecular-scale perspective of association as a function of concentration can inform electrode-solution models at larger scales that capture nonideal solution effects. Even simple salt solutions exhibit significant nonideal behavior at high concentrations. Recent experiments⁶³ and simulations⁶⁴ have shown that extended liquid-like clusters exist in bulk NaCl(aq) at high concentrations, and the extent of these ionic networks is promoted in the double layer at carbon surfaces.²⁹ Since the effectiveness of graphene-electrolyte devices often depends on the ability to “build up the double layer” (i.e., accumulate ions from the bulk solution in the interfacial region), the structure and mobility of ion species can be essential to this.

TABLE I. Electrostatic potential drop ($\Delta\psi$) across the interface (in V), electrochemical double layer capacitance C_{EDL} , quantum capacitance C_Q , and total capacitance C_{TOT} (in $\mu F\ cm^{-2}$) for each concentration considered (in M).

Concentration	$\Delta\psi$	C_{EDL}	C_Q	C_{TOT}
LiCl				
0.5	-0.995	7.20	10.15	4.21
2.0	-0.955	7.50	9.70	4.23
3.0	-0.952	7.52	9.66	4.23
4.0	-0.952	7.52	9.66	4.23
4.4	-0.941	7.61	9.54	4.23
6.0	-0.961	7.45	9.76	4.22
NaCl				
0.5	-0.996	7.19	10.17	4.21
2.0	-0.964	7.43	9.81	4.23
3.0	-0.947	7.56	9.60	4.23
4.0	-0.945	7.58	9.58	4.23
4.4	-0.935	7.66	9.48	4.24
6.0	-0.954	7.51	9.68	4.23
KCl				
0.5	-0.980	7.31	10.07	4.24
2.0	-0.958	7.48	9.73	4.23
3.0	-0.949	7.55	9.62	4.23
4.0	-0.934	7.67	9.46	4.24
4.4	-0.937	7.64	9.50	4.23

1. Ion clusters

Figure 7 provides the average first-sphere coordination number between cations and O of water [see Fig. 7(a)] as well as cations and anions for all systems, calculated using Eq. (2). The results shown in Fig. 7 indicate no significant surface effect on the coordination of cations with water or chloride when ions in the interface ($0 < z < 2.5\ \text{nm}$) and bulk ($2.5 < z < 4.5\ \text{nm}$) regions were investigated. There is a slight increase in the mean cation-anion coordination, and a concomitant decrease in cation-water coordination, at the interface compared to the bulk; however, this difference is within the margin of error. Generally, the effect of increasing concentration is to increase the number of cation-anion contacts, particularly for KCl(aq), where the coordination number is more than double that of the other systems for all concentrations (and with Li-Cl coordination being negligible even at 6 M). From the largest to smallest variation in the coordination number, we can write $K^+ \rightarrow Na^+ \rightarrow Li^+$. This trend follows the decrease of the ion radius and is likely due to the stronger water binding in the solvation spheres of smaller cations. Furthermore, the average cation-water coordination number is unchanging with a concentration within the margin of error.

In simulations of NaCl(aq) in contact with graphite,²⁹ the substrate was found to increase cation-anion correlations in the double layer with respect to the bulk, particularly beyond 5 M. It is important to note that different models (due to the different system) were used and also that system size likely plays a role to the extent

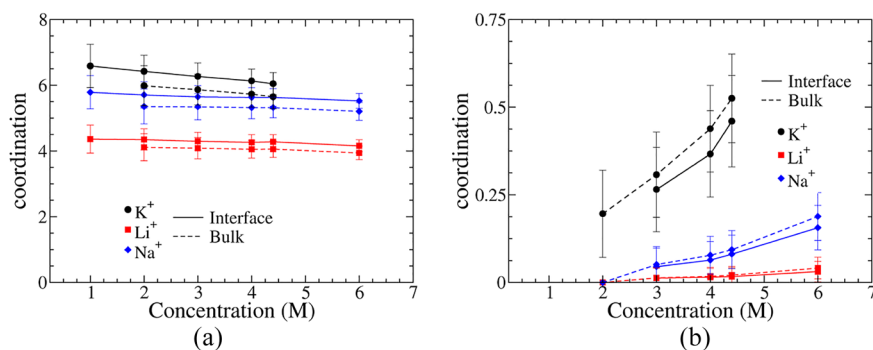


FIG. 7. (a) Cation/water, (b) cation/anion coordination number for the different systems at different concentrations.

that clusters can grow (both in, e.g., the system-size dependence of the availability of ions to form associates and the extent to which finite size and percolating clusters may form in effectively confined canonical systems).

The change in coordination for different salts is reflected in the cluster size probability distributions presented in Fig. 8 for the case of 4.4 M (we report the results for the entire range of concentrations in Fig. S18 of the [supplementary material](#)). There is a clear difference in the extent to which clusters can grow, with lithium forming clusters containing at most four ions and potassium forming much larger networks containing as many as 35 ions. Even at the highest concentrations, the majority of the Li⁺ are dispersed in solution, fully solvated in their first shell. A snapshot of a configuration obtained during the simulation of KCl at 4.4 M is shown in Fig. 8. Although the most probable clusters contain only a few ions (for clusters composed of five ion units, we obtained a relative frequency of 0.01), larger species contribute to the charge storage capacity and must be considered. What we observe is a stronger tendency of the potassium to associate into large aggregates—albeit ones which are highly dynamic on the timescales of the simulations—compared to sodium or lithium.

Since the KCl(aq) system shows the formation of large aggregates of ions, it is interesting to study the relative frequency of the charge of these aggregates. In Fig. 9, we plot the two-dimensional histogram showing the relative frequencies of the charge vs the

cluster size for the KCl(aq) system. The histogram is skewed toward positive charges, with the appearance of clusters containing an excess of positive charge as large as +7e, although the majority of the clusters are neutral.

2. Ion mobilities

As well as a high capacity to store charge, an optimal charge storage device must also be a good electrical conductor. In this regard, it is informative to consider how non-idealities in solution and ion association affect ion conductivities. Here, we determined the conductivity of bulk NaCl(aq) solutions from the ion diffusion coefficients calculated by Finney and Salvalaglio.^{64,65} For this purpose, we use the Nernst–Einstein equation,

$$\sigma_{NE} = \frac{e^2}{Vk_B T} (N_+ z_+^2 D_+ + N_- z_-^2 D_-), \quad (10)$$

where e , V , k_B and T are the elementary charge, simulation cell volume, Boltzmann's constant and temperature, respectively. N and D indicate the total number of ions and the diffusion coefficients for ions with charge indicated by the subscript, respectively. Furthermore, given the highly dynamic nature of the clusters observed in solution, we assume that the valency of ionic species, z , is equal to one.

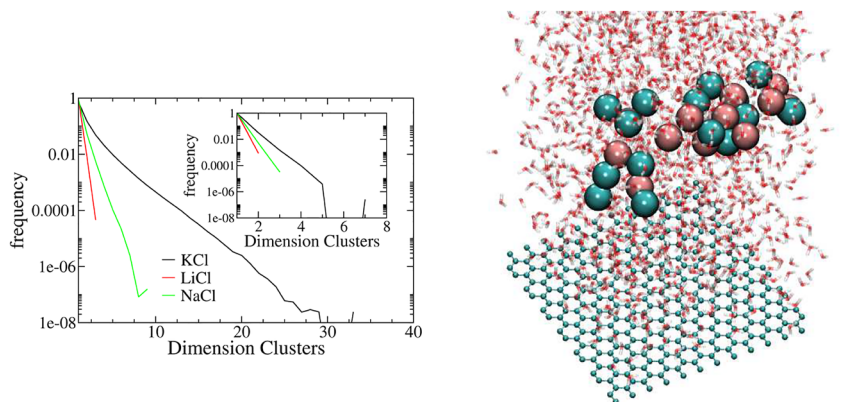


FIG. 8. On the left: Histogram of the relative frequency of the cluster of different sizes for the concentration of 4.4 M. We report the histogram of the relative frequency of the cluster of different sizes for all the concentrations and systems considered in Fig. S18 of the [supplementary material](#). In the inset, the same quantity is reported for the 0.5 M case. On the right: An example of a cluster composed of 26 ions for the KCl system at 4.4 M.

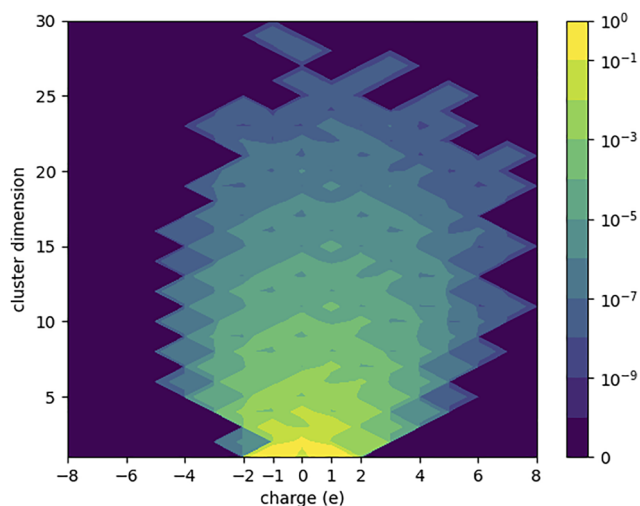


FIG. 9. Two-dimensional histogram (charge vs dimension of the clusters) for the KCl(aq) system at the largest concentration considered (4.4 M).

Suppose we assume that solutions are *ideal*. In that case, we can make use of the mean diffusion coefficient for ions evaluated in the dilute limit (D_{ion}^0) to predict the solution conductivity. For the estimate of D_{ion}^0 , Finney and Salvalaglio⁶⁵ performed extended simulations of a single cation and anion embedded in a simulation cell containing 4000 water molecules; here, $D_+^0 = 1.223 \pm 0.005 \times 10^{-5} \text{ cm}^2 \text{ s}^{-1}$ and $D_-^0 = 1.282 \pm 0.008 \times 10^{-5} \text{ cm}^2 \text{ s}^{-1}$. In addition, the diffusion coefficients were corrected to account for simulation finite size effects.⁶⁶ Unsurprisingly, a linear correlation in σ_{NE} as a function of concentration is found when a constant D_{ion}^0 is used for the diffusion of ions, independent of concentration.

To determine how clustering affects the mobility of the ions and, therefore, the solution conductivity, we analyzed simulations from our previous work⁶⁴ where cubic cells containing 74–370 ions in 1280–4000 water molecules were simulated, providing bulk solution simulations with concentrations in the range 1–10 M. As indicated in Ref. 64, ion association occurred in all simulations. This was significant at the higher end of the concentration range, leading to the formation of large liquid-like ionic networks similar to the KCl clusters described above. Figure 10 also provides the solution conductivities for NaCl(aq) computed using the Nernst–Einstein equation where the mean concentration-dependent diffusion coefficients for ions (D_{ion}) were evaluated using these simulation trajectories. It is important to note that these diffusion coefficients are determined for bulk solutions. There may also be surface effects on the diffusion of ions in the double layer and in bulk solution close to the electrode; nonetheless, this analysis highlights how ion clustering may affect the electrical performance of simple electrolytes at the high end of bulk concentration.

When accounting for the non-idealities in the solution and the formation of clusters explicitly in the diffusion of ions, we find that the solution conductivity reaches an upper limit between 4 and 5 M. At the lowest concentrations (1–2 M), the conductivities determined using D_{ion}^0 and D_{ion} are consistent, and the simulation predictions match well with experimental measurements.⁶⁷ A

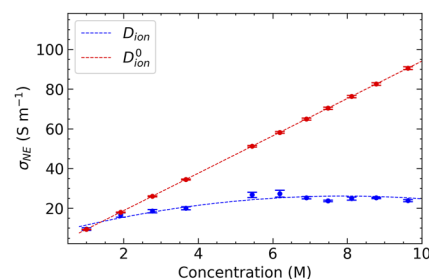


FIG. 10. Solution conductivities, σ_{NE} , of bulk NaCl(aq) solutions calculated for a range of concentrations. To this aim, the Nernst–Einstein equation was adopted where ion diffusion coefficients were determined from simulations at finite concentration, D_{ion} (blue), or from a single simulation at the dilute limit, D_{ion}^0 (red). Dashed lines are a guide for the eye, whereas error bars indicate uncertainties in the conductivities associated with the calculated D value from Refs. 64 and 65.

crossover in the conductivity behavior from the “pseudo-ideal” to nonideal regime occurs between 2 and 3 M. Therefore, over a wide concentration range up to the salt solubility, non-idealities will likely affect the performance of electrical devices; depending upon the chosen application; electrolytes should be selected to minimize these effects.

IV. CONCLUSIONS

In this work, we presented an extended set of simulations describing the interface between three different electrolyte solutions—[KCl(aq), LiCl(aq), and NaCl(aq)]—in contact with the surface of a negatively charged graphene electrode. To investigate these systems, we combined QM/MD and $C\mu$ MD methodologies into a new simulation framework. QM/MD models of the graphene electrode in contact with an electrolyte enabled the explicit coupling of the electrode polarizability with the instantaneous configuration of the electrolyte. The latter was maintained in equilibrium with a liquid phase at constant bulk concentration thanks to the $C\mu$ MD model, which mimics open boundary conditions.

We performed a thorough analysis of the interaction of the ions with the electrode by showing the different behavior of the three cations in the double layer, focusing on K^+ , which, according to our results, can directly adsorb at the electrode surface at shorter distances compared to Li^+ and Na^+ , modifying the screening of the solution.

Calculations of the integral capacitance indicated no concentration dependence or specific ion effects, with a total capacitance of around $4.2 \mu\text{F cm}^{-2}$ across all systems. However, the lack of variation in capacitance hides the rich electrolyte solution behavior, particularly for the ions close to the electrode. We showed, for example, that large KCl clusters emerge in solution, which might be important when considering properties associated with ion mobility and charge transfer.

Our results indicate that accurate models of the interface—able to account for the position-dependent non-ideality of electrolyte solutions—better capture the configurational and dynamical details underpinning the electrochemical behavior of interfaces at the atomistic level, and that is often overshadowed by the calculation of aggregated quantities such as the integral capacitance. We plan to

extend our calculations to include a range of positively and negatively charged electrodes and further investigate ion dynamics in solution.

SUPPLEMENTARY MATERIAL

The [supplementary material](#) includes a report of the numerical values of potential drop in the charged and neutral electrode (see Tables S1 and S2), a sketch of the QMMD part of the model (see Fig. S1), the radial distribution function for cations/anions for all the systems considered (see Fig. S2), the results presented in the paper completed with error bars for all the cases considered (the molar concentrations of cations and anions, Figs. S3–S8; screening factors Figs. S12–S17), the relative frequency of the cluster size (see Fig. S18), the recalculation of the screening factor using all the charges in the electrolyte solution (see Figs. S19–S21), and also the raw data with the charge density in the box for all the systems considered.

ACKNOWLEDGMENTS

We acknowledge the support provided by the IT Services for use of the Computational Shared Facility (CSF) and the University of Manchester. NDP, JDE, and PC thank the European Union's Horizon 2020 research and innovation program project VIMMP under Grant Agreement No. 760907. ARF and MS acknowledge funding from an EPSRC Program Grant (Grant No. EP/R018820/1), which funds the Crystallisation in the Real World consortium.

AUTHOR DECLARATIONS

Conflict of Interest

The authors have no conflicts to disclose.

Author Contributions

Nicodemo Di Pasquale: Conceptualization (lead); Formal analysis (equal); Funding acquisition (equal); Investigation (lead); Methodology (equal); Supervision (lead); Writing – original draft (lead); Writing – review & editing (equal). **Aaron R. Finney:** Conceptualization (equal); Data curation (equal); Investigation (equal); Methodology (equal); Software (supporting); Writing – original draft (equal); Writing – review & editing (supporting). **Joshua Elliott:** Conceptualization (supporting); Data curation (supporting); Investigation (equal); Methodology (equal); Software (supporting); Writing – original draft (supporting); Writing – review & editing (supporting). **Paola Carbone:** Conceptualization (supporting); Formal analysis (equal); Methodology (supporting); Resources (equal); Writing – original draft (supporting); Writing – review & editing (supporting). **Matteo Salvalaglio:** Conceptualization (supporting); Investigation (supporting); Methodology (supporting); Resources (equal); Writing – original draft (supporting); Writing – review & editing (supporting).

DATA AVAILABILITY

The data that support the findings of this study are available from the corresponding author upon reasonable request.

REFERENCES

- 1 D. Cohen-Tanugi and J. C. Grossman, "Water desalination across nanoporous graphene," *Nano Lett.* **12**(7), 3602–3608 (2012).
- 2 M. Heiraniyan, Y. Noh, and N. R. Aluru, "Dynamic and weak electric double layers in ultrathin nanopores," *J. Chem. Phys.* **154**(13), 134703 (2021).
- 3 S. P. Surwade, S. N. Smirnov, I. V. Vlasiouk, R. R. Unocic, G. M. Veith, S. Dai, and S. M. Mahurin, "Water desalination using nanoporous single-layer graphene," *Nat. Nanotechnol.* **10**(5), 459–464 (2015).
- 4 P. Simon and Y. Gogotsi, "Materials for electrochemical capacitors," in *Nanoscience and Technology: A Collection of Reviews from Nature Journals* (World Scientific, 2008), pp. 320–329.
- 5 Y. Wang, L. Zhang, H. Hou, W. Xu, G. Duan, S. He, K. Liu, and S. Jiang, "Recent progress in carbon-based materials for supercapacitor electrodes: A review," *J. Mater. Sci.* **56**(1), 173–200 (2021).
- 6 J. D. Elliott, A. A. Papaderakis, R. A. W. Dryfe, and P. Carbone, "The electrochemical double layer at the graphene/aqueous electrolyte interface: What we can learn from simulations, experiments, and theory," *J. Mater. Chem. C* **10**, 15225–15262 (2022).
- 7 Y. Wang, Z. Shi, Y. Huang, Y. Ma, C. Wang, M. Chen, and Y. Chen, "Supercapacitor devices based on graphene materials," *J. Phys. Chem. C* **113**(30), 13103–13107 (2009).
- 8 C. Liu, Z. Yu, D. Neff, A. Zhamu, and B. Z. Jang, "Graphene-based supercapacitor with an ultrahigh energy density," *Nano Lett.* **10**(12), 4863–4868 (2010).
- 9 A. Yu, I. Roes, A. Davies, and Z. Chen, "Ultrathin, transparent, and flexible graphene films for supercapacitor application," *Appl. Phys. Lett.* **96**(25), 253105 (2010).
- 10 L. L. Zhang, R. Zhou, and X. S. Zhao, "Graphene-based materials as supercapacitor electrodes," *J. Mater. Chem.* **20**(29), 5983–5992 (2010).
- 11 Y. Zhu, S. Murali, M. D. Stoller, K. J. Ganesh, W. Cai, P. J. Ferreira, A. Pirkle, R. M. Wallace, K. A. Cychosz, M. Thommes, D. Su, E. A. Stach, and R. S. Ruoff, "Carbon-based supercapacitors produced by activation of graphene," *Science* **332**(6037), 1537–1541 (2011).
- 12 K. H. An, W. S. Kim, Y. S. Park, Y. C. Choi, S. M. Lee, D. C. Chung, D. J. Bae, S. C. Lim, and Y. H. Lee, "Supercapacitors using single-walled carbon nanotube electrodes," *Adv. Mater.* **13**(7), 497–500 (2001).
- 13 Z. Yang, J. Tian, Z. Yin, C. Cui, W. Qian, and F. Wei, "Carbon nanotube- and graphene-based nanomaterials and applications in high-voltage supercapacitor: A review," *Carbon* **141**, 467–480 (2019).
- 14 C. Merlet, B. Rotenberg, P. A. Madden, and M. Salanne, "Computer simulations of ionic liquids at electrochemical interfaces," *Phys. Chem. Chem. Phys.* **15**(38), 15781–15792 (2013).
- 15 P. Iamprasertkun, W. Hirunpinyopas, A. Keerthi, B. Wang, B. Radha, M. A. Bissett, and R. A. W. Dryfe, "Capacitance of basal plane and edge-oriented highly ordered pyrolytic graphite: Specific ion effects," *J. Phys. Chem. Lett.* **10**(3), 617–623 (2019).
- 16 H. Yang, J. Yang, Z. Bo, X. Chen, X. Shuai, J. Kong, J. Yan, and K. Cen, "Kinetic-dominated charging mechanism within representative aqueous electrolyte-based electric double-layer capacitors," *J. Phys. Chem. Lett.* **8**(15), 3703–3710 (2017).
- 17 Q. T. Qu, B. Wang, L. C. Yang, Y. Shi, S. Tian, and Y. P. Wu, "Study on electrochemical performance of activated carbon in aqueous Li₂SO₄, Na₂SO₄ and K₂SO₄ electrolytes," *Electrochem. Commun.* **10**(10), 1652–1655 (2008).
- 18 J. D. Elliott, A. Troisi, and P. Carbone, "A QM/MD coupling method to model the ion-induced polarization of graphene," *J. Chem. Theory Comput.* **16**(8), 5253–5263 (2020).
- 19 X. Wang, S. M. Tabakman, and H. Dai, "Atomic layer deposition of metal oxides on pristine and functionalized graphene," *J. Am. Chem. Soc.* **130**(26), 8152–8153 (2008).
- 20 M. Gouy, "Sur la constitution de la charge électrique à la surface d'un électrolyte," *J. Phys. Theor. Appl.* **9**(1), 457–468 (1910).
- 21 D. L. Chapman, "II. A contribution to the theory of electrocapillarity," *London, Edinburgh Dublin Philos. Mag. J. Sci.* **25**(148), 475–481 (1913).
- 22 S. Otto, "Zur theorie der elektrolytischen doppelschicht," *Z. Elektrochem. Angew. Phys. Chem.* **30**(21–22), 508–516 (1924).
- 23 M. Popović and A. Šiber, "Lattice-gas Poisson-Boltzmann approach for sterically asymmetric electrolytes," *Phys. Rev. E* **88**(2), 022302 (2013).

- ²⁴I. Borukhov, D. Andelman, and H. Orland, "Steric effects in electrolytes: A modified Poisson-Boltzmann equation," *Phys. Rev. Lett.* **79**(3), 435 (1997).
- ²⁵M. V. Fedorov and A. A. Kornyshev, "Ionic liquid near a charged wall: Structure and capacitance of electrical double layer," *J. Phys. Chem. B* **112**(38), 11868–11872 (2008).
- ²⁶J. J. Howard, J. S. Perkins, and B. M. Pettitt, "The behavior of ions near a charged wall - Dependence on ion size, concentration, and surface charge," *J. Phys. Chem. B* **114**(18), 6074–6083 (2010).
- ²⁷R. P. Misra and D. Blankschtein, "Ion adsorption at solid/water interfaces: Establishing the coupled nature of ion–solid and water–solid interactions," *J. Phys. Chem. C* **125**(4), 2666–2679 (2021).
- ²⁸C. Perego, M. Salvalaglio, and M. Parrinello, "Molecular dynamics simulations of solutions at constant chemical potential," *J. Chem. Phys.* **142**(14), 144113 (2015).
- ²⁹A. R. Finney, I. J. McPherson, P. R. Unwin, and M. Salvalaglio, "Electrochemistry, ion adsorption and dynamics in the double layer: A study of NaCl(aq) on graphite," *Chem. Sci.* **12**(33), 11166–11180 (2021).
- ³⁰K. Doblhoff-Dier and M. T. M. Koper, "Modeling the Gouy–Chapman diffuse capacitance with attractive ion–surface interaction," *J. Phys. Chem. C* **125**(30), 16664–16673 (2021).
- ³¹A. France-Lanord and J. C. Grossman, "Correlations from ion pairing and the Nernst-Einstein equation," *Phys. Rev. Lett.* **122**(13), 136001 (2019).
- ³²R. P. Misra and D. Blankschtein, "Uncovering a universal molecular mechanism of salt ion adsorption at solid/water interfaces," *Langmuir* **37**(2), 722–733 (2021).
- ³³C. D. Williams, J. Dix, A. Troisi, and P. Carbone, "Effective polarization in pairwise potentials at the graphene–electrolyte interface," *J. Phys. Chem. Lett.* **8**(3), 703 (2017).
- ³⁴J. I. Siepmann and M. Sprik, "Influence of surface topology and electrostatic potential on water/electrode systems," *J. Chem. Phys.* **102**(1), 511 (1995).
- ³⁵A. Coretti, C. Bacon, R. Berthin, A. Serva, L. Scalfi, I. Chubak, K. Goloviznina, M. Haefele, A. Marin-Lafleche, B. Rotenberg, S. Bonella, and M. Salanne, "MetalWalls: Simulating electrochemical interfaces between polarizable electrolytes and metallic electrodes," *J. Chem. Phys.* **157**(18), 184801 (2022).
- ³⁶C. Merlet, C. Péan, B. Rotenberg, P. A. Madden, B. Daffos, P.-L. Taberna, P. Simon, and M. Salanne, "Highly confined ions store charge more efficiently in supercapacitors," *Nat. Commun.* **4**(1), 2701 (2013).
- ³⁷C. Merlet, B. Rotenberg, P. A. Madden, P.-L. Taberna, P. Simon, Y. Gogotsi, and M. Salanne, "On the molecular origin of supercapacitance in nanoporous carbon electrodes," *Nat. Mater.* **11**(4), 306–310 (2012).
- ³⁸L. Scalfi, T. Dufils, K. G. Reeves, B. Rotenberg, and M. Salanne, "A semi-classical thomas–fermi model to tune the metallicity of electrodes in molecular simulations," *J. Chem. Phys.* **153**(17), 174704 (2020).
- ³⁹A. Landi, M. Rejsjalali, J. D. Elliott, M. Matta, P. Carbone, and A. Troisi, "Simulation of polymeric mixed ionic and electronic conductors with a combined classical and quantum mechanical model," *J. Mater. Chem. C* (published online) (2023).
- ⁴⁰N. Di Pasquale, J. D. Elliott, P. Hadjidoukas, and P. Carbone, "Dynamically polarizable force fields for surface simulations via multi-output classification neural networks," *J. Chem. Theory Comput.* **17**(7), 4477–4485 (2021).
- ⁴¹M. J. Abraham, T. Murtola, R. Schulz, S. Páll, J. C. Smith, B. Hess, and E. Lindahl, "GROMACS: High performance molecular simulations through multi-level parallelism from laptops to supercomputers," *SoftwareX* **1–2**, 19–25 (2015).
- ⁴²G. A. Tribello, M. Bonomi, D. Branduardi, C. Camilloni, and G. Bussi, "Plumed 2: New feathers for an old bird," *Comput. Phys. Commun.* **185**(2), 604–613 (2014).
- ⁴³B. Hourahine, B. Aradi, V. Blum, F. Bonafé, A. Buccheri, C. Camacho, C. Cavallos, M. Y. Deshayé, T. Dumitrică, A. Dominguez, S. Ehlert, M. Elstner, T. van der Heide, J. Hermann, S. Irle, J. J. Kranz, C. Köhler, T. Kowalczyk, T. Kubař, I. S. Lee, V. Lutsker, R. J. Maurer, S. K. Min, I. Mitchell, C. Negre, T. A. Niehaus, A. M. N. Niklasson, A. J. Page, A. Pecchia, G. Penazzi, M. P. Persson, J. Rezáč, C. G. Sánchez, M. Sternberg, M. Stöhr, F. Stuckenberg, A. Tkatchenko, V. W.-z. Yu, and T. Frauenheim, "DFTB+, a software package for efficient approximate density functional theory based atomistic simulations," *J. Chem. Phys.* **152**(12), 124101 (2020).
- ⁴⁴J. D. Elliott, M. Chiricotto, A. Troisi, and P. Carbone, "Do specific ion effects influence the physical chemistry of aqueous graphene-based supercapacitors? Perspectives from multiscale QMMD simulations," *Carbon* **207**, 292–304 (2023).
- ⁴⁵M. Elstner, D. Porezag, G. Jungnickel, J. Elsner, M. Haugk, T. Frauenheim, S. Suhai, and G. Seifert, "Self-consistent-charge density-functional tight-binding method for simulations of complex materials properties," *Phys. Rev. B* **58**(11), 7260 (1998).
- ⁴⁶W. M. Haynes, D. R. Lide, and T. J. Bruno, *CRC Handbook of Chemistry and Physics* (CRC Press, 2016).
- ⁴⁷I. M. Zeron, J. L. F. Abascal, and C. Vega, "A force field of Li⁺, Na⁺, K⁺, Mg²⁺, Ca²⁺, Cl⁻, and SO₄²⁻ in aqueous solution based on the TIP4P/2005 water model and scaled charges for the ions," *J. Chem. Phys.*, **151**(13):134504, 2019.
- ⁴⁸T. A. Ho and A. Striolo, "Capacitance enhancement via electrode patterning," *J. Chem. Phys.* **139**(20), 204708 (2013).
- ⁴⁹K. Xu, H. Shao, Z. Lin, C. Merlet, G. Feng, J. Zhu, and P. Simon, "Computational insights into charge storage mechanisms of supercapacitors," *Energy Environ. Mater.* **3**(3), 235–246 (2020).
- ⁵⁰R. S. Mulliken, "Electronic population analysis on LCAO–MO molecular wave functions. I," *J. Chem. Phys.* **23**(10), 1833–1840 (1955).
- ⁵¹H. J. C. Berendsen, D. van der Spoel, and R. van Drunen, "Gromacs: A message-passing parallel molecular dynamics implementation," *Comput. Phys. Commun.* **91**(1–3), 43–56 (1995).
- ⁵²D. van der Spoel, E. Lindahl, B. Hess, G. Groenhof, A. E. Mark, and H. J. C. Berendsen, "Gromacs: Fast, flexible and free," *J. Comput. Chem.* **26**(16), 1701–1718 (2005).
- ⁵³H. J. C. Berendsen, J. R. Grigera, and T. P. Straatsma, "The missing term in effective pair potentials," *J. Phys. Chem.* **91**(24), 6269–6271 (1987).
- ⁵⁴S. Miyamoto and P. A. Kollman, "Settle: An analytical version of the SHAKE and RATTLE algorithm for rigid water model," *J. Comput. Chem.* **13**, 952–962 (1992).
- ⁵⁵Y. Huang, J. Liang, and Y. Chen, "An overview of the applications of graphene-based materials in supercapacitors," *Small* **8**(12), 1805–1834 (2012).
- ⁵⁶I. S. Jeong and T. E. Cheatham III, "Determination of alkali and halide monovalent ion parameters for use in explicitly solvated biomolecular simulations," *J. Phys. Chem. B* **112**(30), 9020–9041 (2008).
- ⁵⁷A. Hagberg, P. Swart, and D. S. Chult, in *Exploring Network Structure, Dynamics, and Function Using Networkx* (Los Alamos National Lab. (LANL), Los Alamos, NM, 2008), Technical report.
- ⁵⁸M. F. Döpke, O. A. Moulton, and R. Hartkamp, "On the transferability of ion parameters to the TIP4P/2005 water model using molecular dynamics simulations," *J. Chem. Phys.* **152**(2), 024501 (2020).
- ⁵⁹J. Dočkal, M. Lísal, and F. Moučka, "Molecular dynamics of the interfacial solution structure of alkali-halide electrolytes at graphene electrodes," *J. Mol. Liq.* **353**, 118776 (2022).
- ⁶⁰J. Dockal, F. Moučka, and M. Lísal, "Molecular dynamics of graphene–electrolyte interface: Interfacial solution structure and molecular diffusion," *J. Phys. Chem. C* **123**(43), 26379 (2019).
- ⁶¹A. A. Kornyshev, "Double-layer in ionic liquids: Paradigm change?," *J. Phys. Chem. B* **111**(20), 5545–5557 (2007).
- ⁶²I. Snook and W. van Megen, "Finite ion size effects in the electrical double layer—A Monte Carlo study," *J. Chem. Phys.* **75**(8), 4104–4106 (1981).
- ⁶³H. Hwang, Y. C. Cho, S. Lee, Y.-H. Lee, S. Kim, Y. Kim, W. Jo, P. Duchstein, D. Zahn, and G. W. Lee, "Hydration breaking and chemical ordering in a levitated NaCl solution droplet beyond the metastable zone width limit: Evidence for the early stage of two-step nucleation," *Chem. Sci.* **12**(1), 179–187 (2021).
- ⁶⁴A. R. Finney and M. Salvalaglio, "Multiple pathways in NaCl homogeneous crystal nucleation," *Faraday Discuss.* **235**, 56–80 (2022).
- ⁶⁵A. R. Finney and M. Salvalaglio, "Bridging the gap between mesoscopic and molecular models of solid/liquid interfaces out-of-equilibrium," *Chem. Eng. Res. Design* **180**, 285–295 (2022).
- ⁶⁶I.-C. Yeh and G. Hummer, "System-size dependence of diffusion coefficients and viscosities from molecular dynamics simulations with periodic boundary conditions," *J. Phys. Chem. B* **108**(40), 15873–15879 (2004).
- ⁶⁷C. S. Widodo, H. Sela, and D. R. Santosa, "The effect of NaCl concentration on the ionic NaCl solutions electrical impedance value using electrochemical impedance spectroscopy methods," *AIP Conf. Proc.* **2021**, 050003 (2018).